

₁ Study of neutrino-nucleus interaction at around 1 GeV using
₂ hollow cuboid lattice neutrino detectors, WAGASCI, muon
₃ range detectors and magnetized spectrometer, Baby MIND,
₄ at J-PARC neutrino monitor hall

₅ A. Bonnemaison, R. Cornat, L. Domine, O. Drapier, O. Ferreira, F. Gastaldi,
₆ M. Gonin, J. Imber, M. Licciardi, F. Magniette, T. Mueller, L. Vignoli, and O. Volcy

₇ *Ecole Polytechnique, IN2P3-CNRS, Laboratoire Leprince-Ringuet, Palaiseau,*
₈ *France*

₉ S. Cao and T. Kobayashi

₁₀ *High Energy Accelerator Research Organization (KEK), Tsukuba, Ibaraki, Japan*

₁₁ M. Khabibullin, A. Khotjantsev, A. Kostin, Y. Kudenko, A. Mefodiev, O. Mineev,
₁₂ S. Suvorov, and N. Yershov

₁₃ *Institute for Nuclear Research of the Russian Academy of Sciences, Moscow, Russia*

₁₄ B. Quilain

₁₅ *Kavli Institute for the Physics and Mathematics of the Universe (WPI), The*
₁₆ *University of Tokyo Institutes for Advanced Study, University of Tokyo, Kashiwa,*
₁₇ *Chiba, Japan*

₁₈ T. Hayashino, A. Hiramoto, A.K. Ichikawa, K. Nakamura, T. Nakaya, K Yasutome,
₁₉ and K. Yoshida

₂₀ *Kyoto University, Department of Physics, Kyoto, Japan*

₂₁ Y. Azuma, J. Harada, T. Inoue, K. Kin, N. Kukita, S. Tanaka, Y. Seiya,
₂₂ K. Wakamatsu, and K. Yamamoto

₂₃ *Osaka City University, Department of Physics, Osaka, Japan*

24 A. Blondel, F. Cadoux, Y. Favere, E. Noah, L. Nicola, and S. Parsa

25 *University of Geneva, Section de Physique, DPNC, Geneva, Switzerland*

26 N. Chikuma, F. Hosomi, T. Koga, R. Tamura, and M. Yokoyama

27 *University of Tokyo, Department of Physics, Tokyo, Japan*

28 Y. Hayato

29 *University of Tokyo, Institute for Cosmic Ray Research, Kamioka Observatory,*
30 *Kamioka, Japan*

31 Y. Asada, K. Matsushita, A. Minamino, K. Okamoto, and D. Yamaguchi

32 *Yokohama National University, Faculty of Engineering, Yokohama, Japan*

33 December 14, 2017

34 **Contents**

35	1	Introduction	3
36	2	Experimental Setup	4
37	2.1	WAGASCI modules	5
38	2.1.1	Detector	5
39	2.1.2	Electronics	8
40	2.1.3	Water system	9
41	2.2	INGRID Proton module	10
42	2.3	Baby MIND	11
43	2.3.1	Magnet modules	11
44	2.3.2	Scintillator modules	12
45	2.3.3	Electronics	14
46	2.3.4	Pefromance check	15
47	2.4	Side muon range detector	15

48	3 Physics goals	18
49	3.1 Expected number of events	19
50	3.2 Pseudo-monochromatic beam by using different off-axis fluxes	19
51	3.3 Subjects WAGASCI can contribute	20
52	4 Status of J-PARC T59 experiment	22
53	5 MC studies	26
54	5.1 Simulation setup	26
55	5.2 Event selection	27
56	6 Standalone WAGASCI-module performances	28
57	6.1 Reconstruction algorithm	30
58	6.1.1 Description	30
59	6.1.2 Performances	32
60	6.2 Background subtraction: the water-out module	36
61	7 Schedule	39
62	8 Requests	39
63	8.1 Neutrino beam	39
64	8.2 Equipment request including power line	39

65 **1 Introduction**

66 The understanding of neutrino-nucleus interactions in the 1 GeV energy region is critical
 67 for the success of accelerator-based neutrino oscillation experiments such as the T2K exper-
 68 iment. Complicated multi-body effects of nuclei render this understanding difficult. The
 69 T2K near detectors have been measuring these and significant progress has been achieved.
 70 However, the understanding is still limited. One of the big factors preventing a complete
 71 understanding is the non-monochromatic neutrino beam spectrum. Measurements with
 72 distinct but partially overlapping beam spectra would be a great benefit in resolving the
 73 contribution from different neutrino energies. We, the WAGASCI collaboration, proposes
 74 to study the neutrino-nucleus interaction at the B2 floor of the neutrino monitor building,
 75 where different neutrino spectra from the T2K off-axis near detector (ND280) can be ob-
 76 tained due to the different off-axis position. Our experimental setup contains two hollow
 77 cuboid lattice detectors as the neutrino interaction target (known as WAGASCI modules),
 78 two side- and one downstream- muon range detectors(MRD's). We will have two types of
 79 the WAGASCI modules, a water-in module and a water-out module. The water-in WA-
 80 GASCI module has water the hollow cuboid lattice, and the water-out WAGASCI module
 81 doesn't have water inside the lattice. The hollow cuboid lattice and side-MRD's allow a

82 measurement of wider-angle scattering than ND280. High water to scintillator material
83 ratio enables the measurement of the neutrino interaction with water, which is highly de-
84 sired for the T2K experiment because it's far detector, Super-Kamiokande, is composed of
85 water. The MRD's consist of plastic scintillators and iron plates. The downstream-MRD,
86 so called the Baby MIND detector, also works as a magnet and provides the charge iden-
87 tification capability as well as magnetic momentum measurement for high energy muons.
88 The charge identification is essentially important to select antineutrino events in the an-
89 tineutrino beam because contamination of the neutrino events is as high as 30%. Most of
90 the detectors have already been constructed. The WAGASCI modules have been commis-
91 sioned as the J-PARC T59 experiment and the Baby MIND detector was commissioned at
92 the CERN neutrino platform. Therefore, the collaboration will be ready to proceed to the
93 physics data taking for the T2K beam time in January 2019. We will provide the cross sec-
94 tions of the charged current neutrino and antineutrino interactions on water with slightly
95 higher neutrino energy than T2K ND280 with wide angler acceptance. When combined
96 with ND280 measurements, our measurement would greatly improve the understanding
97 of the neutrino interaction at around 1 GeV and contribute to reducing one of the most
98 significant uncertainties of the T2K experiment.

99 2 Experimental Setup

100 Figure 1 and 2 show a schematic view and a CAD drawing of the entire set of detectors.
101 Central neutrino target detectors consist of two WAGASCI modules and T2K INGRID
102 proton module. Inside the WAGASCI module, plastic scintillator bars are aligned as a
103 hollow cuboid lattice and spaces in the lattice are filled with water for a water-in WAGASCI
104 module. T2K INGRID proton module is a full active neutrino target detector which is
105 composed only with scintillator bars in its tracking region. The central detectors are
106 surrounded by two side- and one downstream- muon range detectors(MRD's) The MRD's
107 are used to select muon tracks from the charged-current (CC) interactions and to reject
108 short tracks caused by neutral particles that originate mainly from neutrino interactions in
109 material surrounding the central detector, like the walls of the detector hall, neutrons and
110 gammas, or neutral-current (NC) interactions. The muon momentum can be reconstructed
111 from its range inside the detector. The MRD's consist of plastic scintillators and iron plates.
112 The downstream-MRD, also known as the Baby MIND detector, additionally has a coil
113 wound around each of the iron plates so it may be magnetized. This provides the charge
114 selection capability.

115 For all detectors, scintillation light in the scintillator bar is collected and transported
116 to a photodetector with a wavelength shifting fiber (WLS fiber). The light is read out by
117 a photodetector, Multi-Pixel Photon Counter (MPPC), attached to one end of the WLS
118 fiber. The signal from the MPPC is read out by the dedicated electronics developed for
119 the test experiment to enable bunch separation in the beam spill. The readout electronics

120 are triggered using the beam-timing signal from MR to synchronize to the beam. The
121 beam-timing signal is branched from those for T2K, and will not effect T2K data taking.

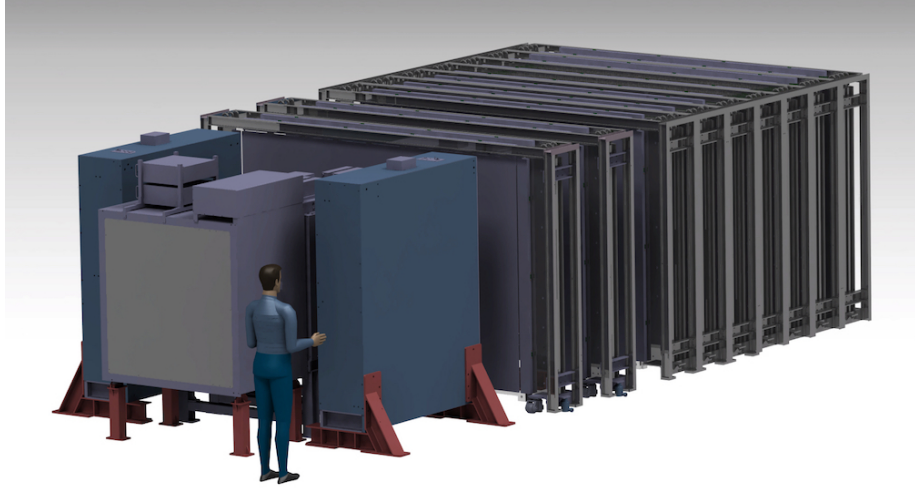


Figure 1: Schematic view of entire sets of detectors.

122 T2K adopted the off-axis beam method, in which the neutrino beam is intentionally
123 directed 2.5 degrees away from SK producing a narrow band ν_μ beam. The off-axis near
124 detector, ND280, is installed towards the SK direction in the B1 floor of the near detector
125 hall of the J-PARC neutrino beam-line. We propose to install our detector in the B2 floor
126 of the near detector hall, where the off-axis angle of 1.5 degrees is slightly different to the
127 2.5 degrees of ND280. The candidate detector position in the B2 floor is shown in Figure
128 3. The expected neutrino energy spectrum at the candidate position is shown in Figure 4.

129 **2.1 WAGASCI modules**

130 **2.1.1 Detector**

131 The WAGASCI modules are mainly composed of 1280 plastic scintillator bars and a sur-
132 rounding stainless steel tank as shown in Figure 5. The total number of channels in one
133 WAGASCI module is 1280. The stainless steel tank is constructed by welding stainless
134 steel plates, is sized as 460mm×1250mm×1250 mm, and weighs 0.5 tonne.

135 One WAGASCI module consists of 16 scintillator tracking planes, where each plane
136 is an array of 80 scintillator bars fixed with ABS frames. The 40 bars, called parallel
137 scintillators, are placed perpendicularly to the beam, and the other 40 bars, called lattice
138 scintillators, are placed in parallel to the beam with hollow cuboid lattice in the tracking
139 plane as shown in Figure 5. Thanks to the hollow cuboid lattice of the scintillator bars,

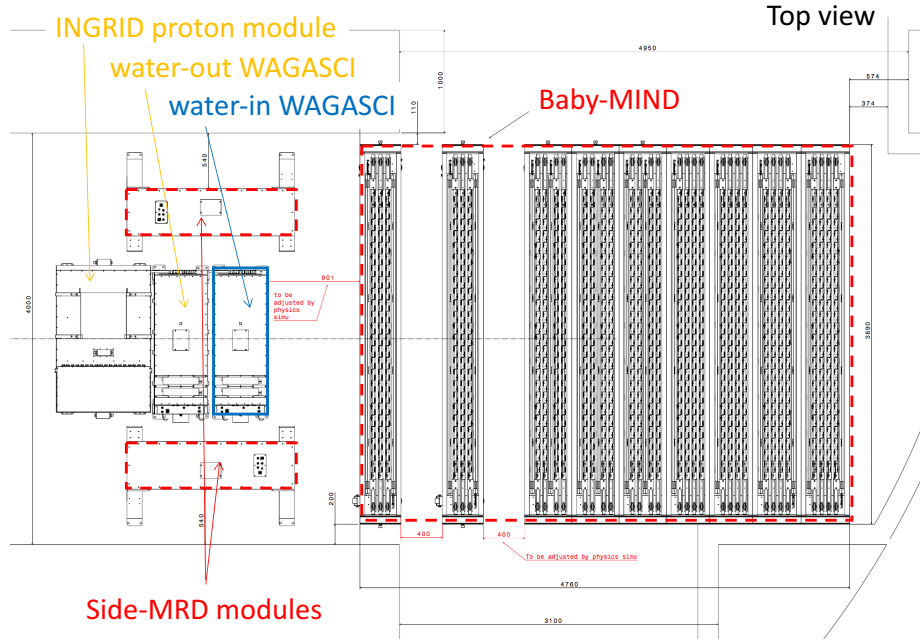


Figure 2: Top view of entire sets of detectors.

140 the WAGASCI module has 4π angular acceptance for charged particles.

141 Thin plastic scintillator bars produced at Fermilab by extrusion method, mainly consists
 142 of polystyrene and are surrounded by thin reflector including TiO^2 (3 mm in thickness)
 143 are used for the WAGASCI modules to reduce the mass ratio of scintillator bars to water,
 144 because neutrino interactions in the scintillator bars are a background for the cross section
 145 measurements on H_2O . Each scintillator bar is sized as $1020\text{mm} \times 25\text{mm} \times 3$ mm including
 146 the reflector part, and half of all the scintillator bars have 50-mm-interval slits to form the
 147 hollow cuboid lattice (Figure 6).

148 We will have two types of the WAGASCI modules, a water-in module and a water-out
 149 module. The water-in WAGASCI module has water in spaces of the hollow cuboid lattice.
 150 The total water mass serving as neutrino targets in the fiducial volume of the module is
 151 188 kg, and the mass ratio of scintillator bars to water is 80 %. The water-out WAGASCI
 152 module doesn't have water inside the detector. The total CH mass serving as neutrino
 153 target in the fiducial volume of the module is 47 kg, and the mass fraction of scintillator
 154 bars is 100 %.

155 Scintillation light is collected by wave length shifting fibers, Y-11 (non-S type with a
 156 diameter of 1.0 mm produced by Kuraray. A fiber is glued by optical cement in a groove
 157 on surface of a scintillator bar. 32 fibers are gathered together by a fiber bundle at edge

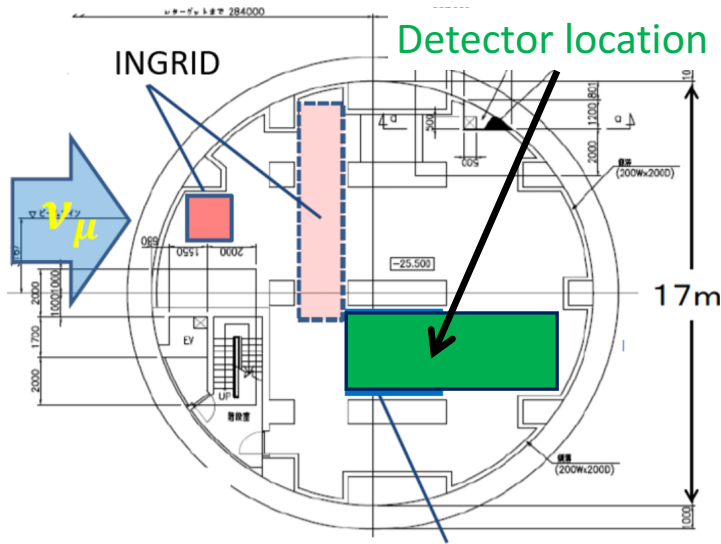


Figure 3: Candidate detector position on the B2 floor of the near detector hall.

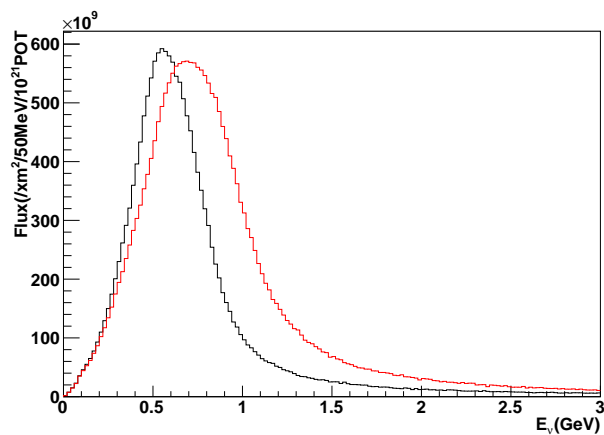


Figure 4: Neutrino energy spectrum at the candidate detector position (red, off-axis 1.5 degree). The spectrum at the ND280 site (black, off-axis 2.5 degree) is also shown.

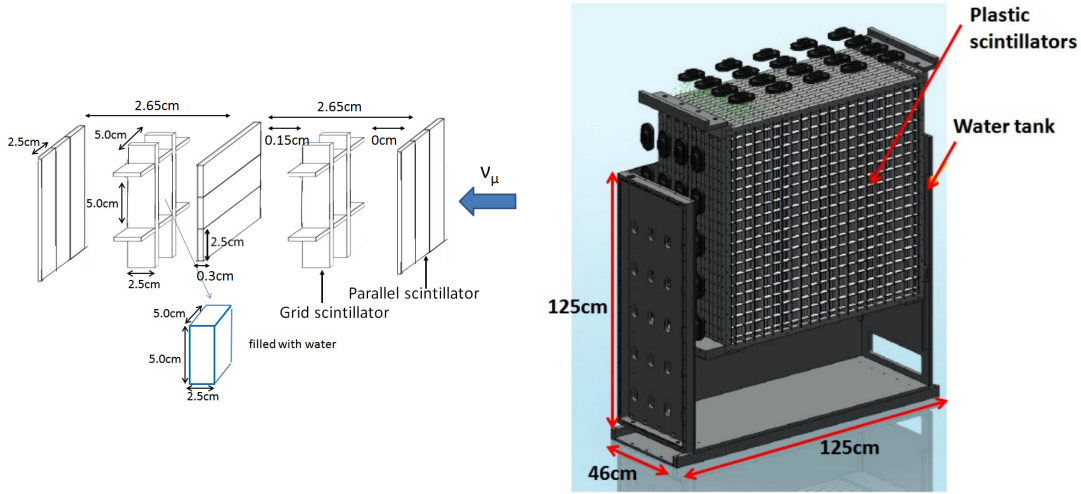


Figure 5: Schematic views of hollow cuboid lattice of plastic scintillator bars (left) and WAGASCI module (right).

of the module, and lead scintillation light to a 32-channel arrayed MPPC. Since crosstalk of light yield due to reflection on the inner surface of each cell has been observed, all the scintillator bars are painted black by aqueous color spray. It is confirmed by measurements with cosmic rays that black painting on the surface of the scintillator bars suppresses this crosstalk so that no significant crosstalk effect is observed within uncertainty.

32-channel arrayed MPPCs, as shown in the Figure 7, are used for the modules. The surface of the fiber bundle is polished and directly attached onto the 32-channel arrayed MPPCs. The positions of 32 fibers on the bundle are aligned to fit the channels of MPPCs. The MPPC is a product of Hamamatsu Photonics, S13660(ES1), with suppressed noise rate of ~ 6 kHz per channel at 0.5 p.e. threshold. For each MPPC channel, 716 pixels of APD are aligned in a shape of circle.

2.1.2 Electronics

As front-end electronics of this detector, a Silicon PM Integrated Read-Out Chip (SPIROC) [11] is adopted. SPIROC is a 36-channel auto-triggered front-end ASIC, and is produced by OMEGA/ IN2P3. It not only contains an analog signal processing part such as amplification and shaping of the waveform, but contains a digital signal processing parts such as auto-trigger and timing measurement. Charge of MPPC signal is sampled by track-and-hold circuit. A Front-end electronics board, Active Sensor Unit (ASU), has been developed with the SPIROC2D chip, which is the latest version of SPIROC. Each readout board is designed to control a 32-channel arrayed MPPC, and 40 of the ASU boards are aligned on

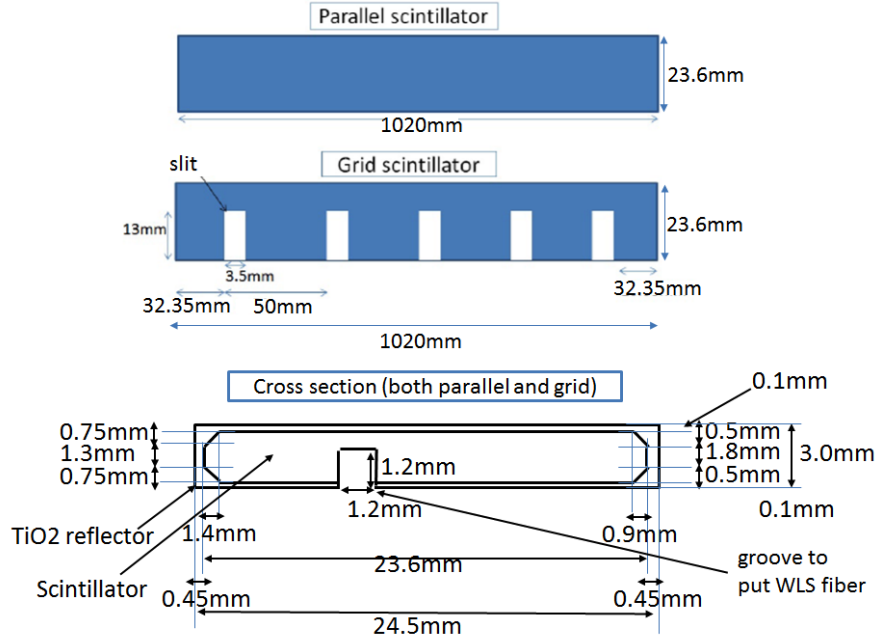


Figure 6: Geometry of scintillators used for WAGASCI modules.

178 the module surface. The data acquisition system used for this detector, including back-end
 179 boards, has been developed for prototypes of ultra-granular calorimeters for the Interna-
 180 tional Linear Collider (ILC) [4], and independent of the T2K DAQ system. To synchronize
 181 the DAQ system to J- PARC neutrino beam, pre-beam trigger and beam trigger are sent to
 182 the clock control card. The beam trigger signals are converted from optical signals to NIM
 183 signals at NIM module on the B2 floor. In addition, the information of spill number are
 184 delivered with 16-bit ECL level signals, and converted to an Ethernet frame by an FPGA
 185 evaluation board to be directly sent to the DAQ PC. The electronics readout scheme is
 186 shown in Figure 8.

187 2.1.3 Water system

188 Pure water is filled to the water tank of the water-in WAGASCI module as follows. First,
 189 the water storage tank located at the B2 floor of the NM pit is filled with water delivered
 190 from a water tap on the ground level through a long hose. Second, the water is pumped
 191 to the other water storage tank though a water filler to produce pure water. Third, a
 192 compound preservative called Germall plus, which is the same preservative used in one of
 193 the sub-detectors of T2K ND280, FGD2, is put into the water to keep water from being
 194 bad. Then, the water is poured to the water-in WAGASCI module, and it is kept in the

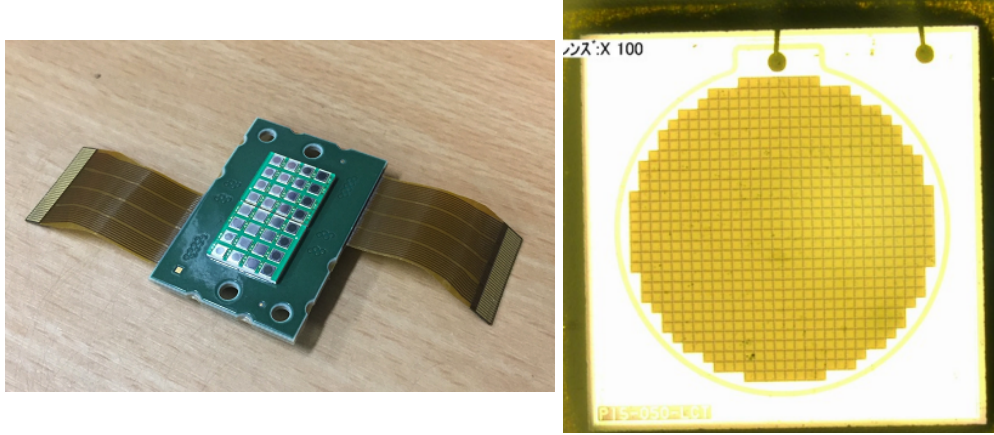


Figure 7: 32-channel arrayed MPPC (left) and an enlarged view of one MPPC channel (right).

195 module during the neutrino beam operation and not to be circulated.

196 2.2 INGRID Proton module

197 INGRID Proton module is a neutrino detector of the T2K experiment. It is a fully-active
198 tracking detector which consists of only scintillator strips. The purpose of this Proton
199 Module is to separate the neutrino interaction types by detecting the protons and pions
200 together with the muons from the neutrino interactions, and to measure the neutrino cross
201 section for each interaction type. It consists of 36 tracking planes surrounded by veto
202 planes (Figure 9), where each tracking plane is an array of two types of scintillator strips.
203 The 16 strips in the inner region have dimensions of $25\text{mm} \times 13\text{mm} \times 1200\text{mm}$, while the 16
204 strips in the outer region have dimensions of $50\text{mm} \times 10\text{mm} \times 1200\text{mm}$, making a plane of
205 $1200\text{mm} \times 1200\text{mm}$ in the horizontal and vertical directions. The former is the scintillator
206 produced for the K2K SciBar detector [3] and the latter was produced for INGRID. The
207 tracking planes are placed perpendicular to the beam axis at 23mm intervals. Since the
208 strips are aligned in one direction, each tracking plane is sensitive to either the horizontal or
209 vertical position of the tracks. The tracking planes are therefore placed alternating in the
210 horizontal and vertical directions so that three-dimensional tracks can be reconstructed.
211 The tracking planes also serve as the neutrino interaction target. As with the WAGASCI
212 modules, scintillation light is read out by a WLS fiber and MPPC.

213 It was installed on the neutrino beam axis on the SS floor of the T2K near detector hall
214 in 2010, and had been used for neutrino cross section measurements. In August 2017, it
215 was moved to the B2 floor of the T2K near detector hall by J-PARC T59 after getting the
216 approval from T2K to use them. J-PARC T59 is performing a neutrino beam measurement

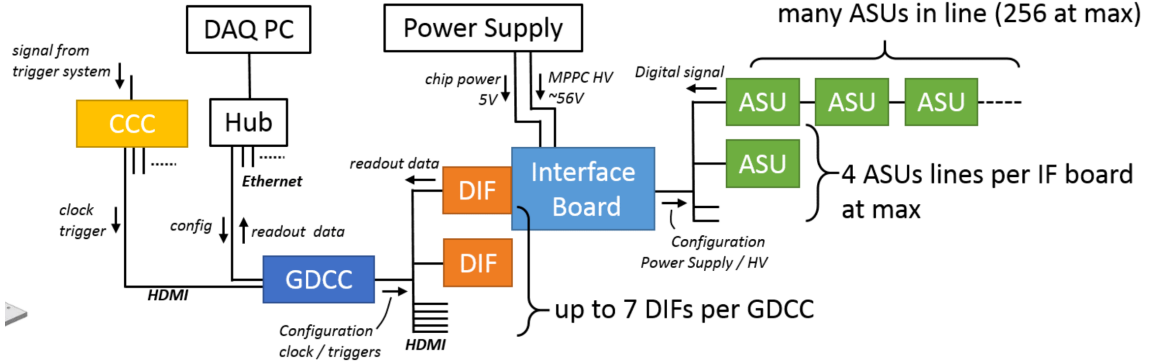


Figure 8: WAGASCI electronics readout scheme.

217 using the detector from October 2017, and the measurement will continue until May 2018
 218 as we will discuss in Sec. 4.

219 We will operate the INGRID Proton module using the T2K near detector electronics/
 220 DAQ system in the same way as J-PARC T59. A proposal to use the module and its
 221 electronics for our project will be submitted to the T2K collaboration.

222 2.3 Baby MIND

223 The Baby MIND is the downstream Muon Range Detector. It also works as a magnet and
 224 provides the charge identification capability as well as magnetic momentum measurement
 225 for high energy muons.

226 The Baby MIND collaboration ¹ submitted a proposal to the SPSC at CERN, SPSC-P-
 227 353. The project was approved by the CERN research board as Neutrino Platform project
 228 NP05 and constructed. The detector consists of 33 magnet modules, each 3500 mm ×
 229 2000 mm × 50 mm (30 mm steel) with a mass of approximately 2 tonnes. Of these magnet
 230 modules, 18 are instrumented with plastic scintillator modules.

231 2.3.1 Magnet modules

232 Traditional layouts for magnetized iron neutrino detectors (e.g. MINOS) tend to be mono-
 233 lithic blocks with a unique pitch between consecutive steel segments and large conductor
 234 coils threaded around the whole magnet volume. The Baby MIND detector, like traditional
 235 designs, is built from sheets of iron interleaved with scintillator detector modules. However
 236 Baby MIND is novel in that the iron segments are all individually magnetized as shown in
 237 Figure 10, allowing for far greater flexibility in the setting of the pitch between segments,
 238 and in the allowable geometries that these detectors can take.

¹Contact person: E. Noah, Spokesperson: A. Blondel, Deputy spokesperson: Y. Kudenko



Figure 9: Schematic view of INGRID Proton module.

239 The key design outcome is a highly optimized magnetic field map. A double-slit con-
 240 figuration for coil winding was adopted to increase the area over which the magnetic flux
 241 lines are homogeneous in B_x across the central tracking region. Simulations show the
 242 magnet field map to be very uniform over this central tracking region covering an area of
 243 $2800 \times 2000 \text{ mm}^2$, Figure 11. The B_x component dominates in this region, with negligible
 244 B_y and B_z . This was confirmed by measuring the field with 9 pick-up coils wound around
 245 the first module. Subsequent modules were equipped with one pick-up coil. Test results
 246 on the 33 modules show all achieve the required field of 1.5 T for a current of 140 A, with
 247 a total power consumption of 11.5 kW. The polarity of the field map shown in Figure 11
 248 (middle) can be reversed by changing the power supply configuration.

249 **2.3.2 Scintillator modules**

250 Each of the 18 scintillator modules is constructed from 2 planes of horizontal counters (95
 251 counters in total) and 2 planes of vertical counters (16 counters in total) [2], arranged
 252 with an overlap between planes to achieve close to 100% hit efficiency for minimum ioniz-
 253 ing muons. The arrangement of planes within a module is vertical-horizontal-horizontal-
 254 vertical. This arrangement was the result of an assembly approach whereby each plane
 255 was built from 2 half-planes, with each half plane consisting of a horizontal plane and a
 256 vertical plane. The scintillator bars are held in place using structural ladders that align
 257 and maintain the counters, Figure 12. No glue is used in the process, so counters can be
 258 replaced. Aluminum sheets front and back provide light tightness.

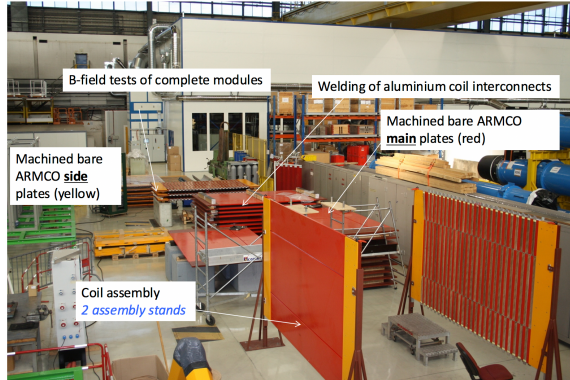


Figure 10: Magnet assembly zone at CERN.

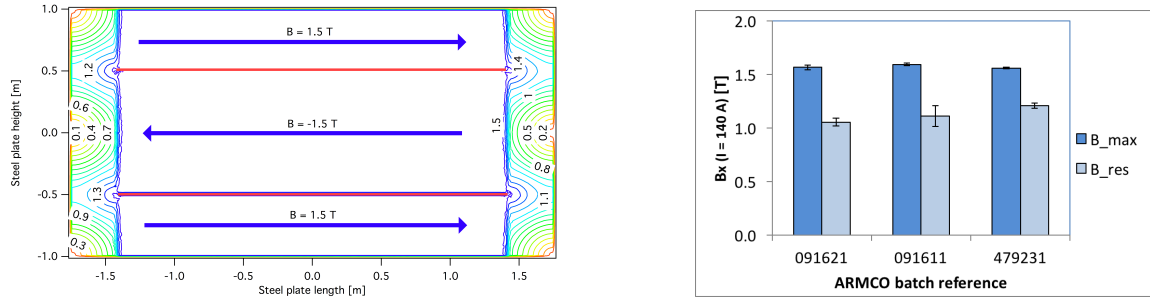


Figure 11: Left) Magnetic field map with a coil along 2800 mm of the length of the plate. Right) Measured B field for 33 modules.



Figure 12: Scintillator modules assembly. Left) top of front half-module showing vertical counters, and the spacer-ladders that set the pitch between horizontal counters and hold them in place. Middle) rear half-module showing horizontal counters on their ladders. Right) Assembled rear half-module, the front half-module can be seen in the background.

259 The plastic scintillator counters were made from 220 mm-wide slabs, consisting of
 260 extruded polystyrene doped with 1.5% paraterphenyl (PTP) and 0.01% POPOP. They were
 261 cut to size then covered with a 30-100 μm thick diffuse reflector resulting from etching of
 262 the surface with a chemical agent [8, 9]. The horizontal counter size is $2880 \times 31 \times 7.5 \text{ mm}^3$,
 263 with one groove along the length of the bar in which sits a wavelength shifting fiber from
 264 Kuraray. The vertical counter size is $1950 \times 210 \times 7.5 \text{ mm}^3$, with one U-shaped groove
 265 along the bar. On each counter, two custom connectors house silicon photomultipliers,
 266 MPPC type S12571-025C from Hamamatsu, either side of the horizontal counter, and
 267 both connectors at the top for the vertical counter. This geometrical configuration for
 268 vertical counters was chosen for ease of connectivity to the electronics, and maintenance
 269 operations.

270 A total of 1744 horizontal counters and 315 vertical counters (including spares) were
 271 produced at the Uniplast company (Vladimir, Russia).

272 2.3.3 Electronics

273 The Baby MIND electronic readout scheme includes several custom-designed boards [10].
 274 The revised version is shown in Figure 13. At the heart of the system is the electronics
 275 Front End Board (FEB), developed by the University of Geneva. The readout system
 276 includes two ancillary boards, the Backplane, and the Master Clock Board (MCB) whose
 277 development has been managed by INRNE (Bulgarian Academy of Sciences) collaborators.

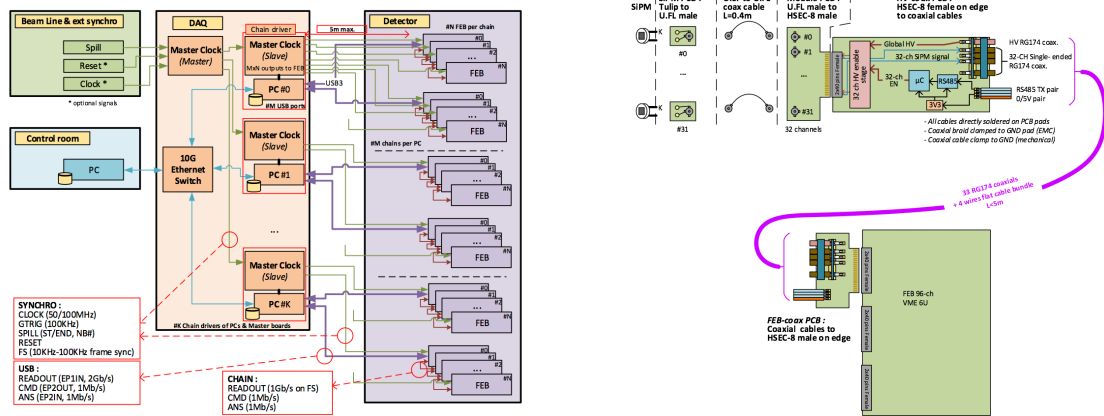


Figure 13: Left) Baby MIND electronics readout scheme. Right) SiPM-to-FEB connectivity.

278 The FEBv2 hosts 3 CITIROC chips that can each read in signals from 32 SiPMs [5].
 279 Each signal input is processed by a high gain (HG), and a separate low gain (LG), signal
 280 path. The outputs from the slow shapers can be sampled using one of two modes: a
 281 mode with an externally applied delay, and a peak detector mode. A faster shaper can be

switched to either HG or LG paths, followed by discriminators with adjustable thresholds providing 32 individual trigger outputs and one OR32 trigger output. An Altera ARIA5 FPGA on the FEBv2 samples these trigger outputs at 400 MHz, recording rising and falling times for the individual triggers and assigning time stamps to these. Time-over-threshold, the difference between falling and rising times, gives some measure of signal amplitude. This is used in addition to charge information and proves useful if there is more than one hit per bar within the $\sim 9 \mu\text{s}$ deadtime due to the readout of the multiplexed charge output. The ARIA5 also manages the digitization of the sampled CITIROC multiplexed HG and LG outputs via a 12-bit 8-ch ADC.

The internal 400 MHz clock on the FEBv2 can be synchronized to a common 100 MHz clock. The synchronization subsystem combines input signals from the beam line into a digital synchronization signal (SYNC) and produces a common detector clock (CLK) which can eventually be synchronised to an external experiment clock. Both SYNC and CLK signals are distributed to the FEBs. Tests show the FEB-to-FEB CLK(SYNC) delay difference to be 50 ps (70 ps). Signals from the beam line at WAGASCI include two separate timing signals, arriving 100 ms and 30 μs before the neutrino beam at the near detectors. The spill number is available as a 16-bit signal.

2.3.4 Pefromance check

All counters were measured at INR Moscow with a cosmic ray setup using the same type S12571-025C MPPCs and a CAEN DT5742 digitizer. The average light yield (sum from both ends) was measured to be 37.5 photo-electrons (p.e.) per minimum ionizing particle (MIP) and 65 p.e./MIP for vertical and horizontal counters, respectively. After shipment to CERN, all counters were individually re-tested with an LED [?]. 0.1% of counters failed the LED tests and were therefore not used during the assembly of modules. The assembly of modules was completed in June 2017, and it was then tested in June and July 2017 at the Proton Synchrotron experimental hall at CERN with a mixed particle beam comprising mostly muons whose momenta could be selected between 0.5 and 5 GeV/c. An event display from the summer 2017 tests is shown in Figure 14.

2.4 Side muon range detector

Two Side-MRD modules for tracking secondary particles from neutrino interactions will be installed in 2018. Each Side-MRD module is composed of 11 steel plates and 80 scintillator slabs. The slabs are arranged as 10 layers installed in the 13 mm gaps between the 30 mm thick plates. Each steel plate size is 30 mm \times 1610 mm \times 1800 mm. Total module size is 2236 mm \times 1630 mm \times 975 mm as shown in Figure 15 (left), weight is \sim 8.5 tonne.

Scintillator bars were manufactured by Uniplast company in Vladimir, Russia. Polystyrene based scintillators were extruded with thickness of 7 mm, then cut to the size of 7 \times 200 \times 1800 mm³. Dopant composition is 1.5% PTP and 0.01% POPOP. Scintillator surface was

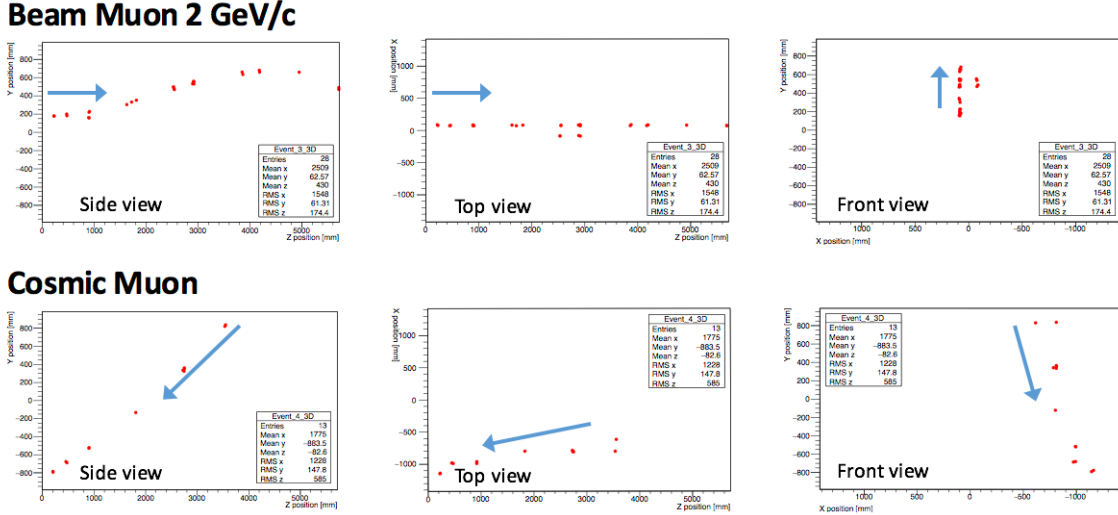


Figure 14: Comparison of a beam muon and cosmic muon in the three different geometrical projections of the detector. The beam impinges on the detector from the left. The arrows indicate the direction of travel of these muons. The direction of the cosmic muon is inferred from timing information.

319 etched by a chemical agent to form a white diffuse layer with excellent reflective performance.
 320 Ideal contact between the scintillator and the reflector raises the light yield up
 321 to 50% comparing to an uncovered scintillator. A sinusoidal groove was milled along the
 322 scintillator to provide uniform light collection over the whole scintillator surface. WLS Y11
 323 Kuraray fiber of 1 mm diameter was glued with an optical cement EJ-500 in the S-shape
 324 groove as shown in Figure 15(right). A minimum bending radius of 30 mm was used to
 325 ensure the the Kuraray S-type fibers remained within specification. Both ends of the fiber
 326 were glued into optical connectors which were themselves attached to the scintillator and
 327 provide an interface to SiPMs, Hamamatsu MPPC S13081-050CS(X1).

328 Scintillators for the Side-MRD modules were assembled at INR in Russia, and shipped
 329 to Japan in July 2017. The light yield for each scintillator was measured with cosmic
 330 rays at INR and at YNU in Japan after delivery. LY_1 and LY_2 are light yields measured
 331 at both ends of the counter. The light yield asymmetry between the ends calculated as
 332 $100\% \times \frac{LY_1 - LY_2}{LY_1 + LY_2}$. After tests at INR we selected 324 counters from measured 332 ones with
 333 the mean light yield of 45 p.e./MIP ($LY_1 + LY_2$) and the asymmetry value less than 10
 334 %. The measuremens at YNU yielded the average total light yield of about 40 p.e./MIP
 335 which varies in range from 32 to 50 p.e./MIP (Figure 16 (left)). Only two counters showed
 336 relatively high asymmetry close to 25 % as shown in Figure 16 (right). Using the results of
 337 the quality assurance test we selected 320 scintillator counters for the Side-MRD modules.

338 We also measured the time resolution for a combination of four counters piled one

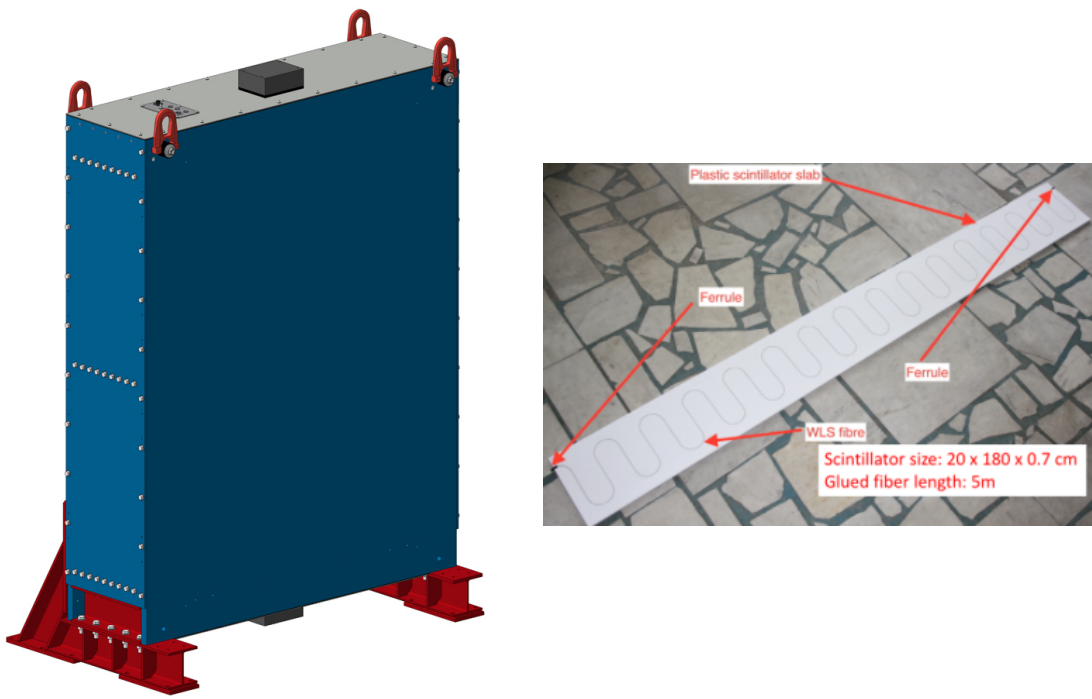


Figure 15: Left :Side-MRD module. Right: Scintillator bar of the Side-MRD modules.

upon another. The average result for four counters is $\sigma_T = 1.04$ ns. The resolution of combination of 2, 3, 4 counters is measured to be 0.79 ns, 0.66 ns and 0.58 ns, respectively.

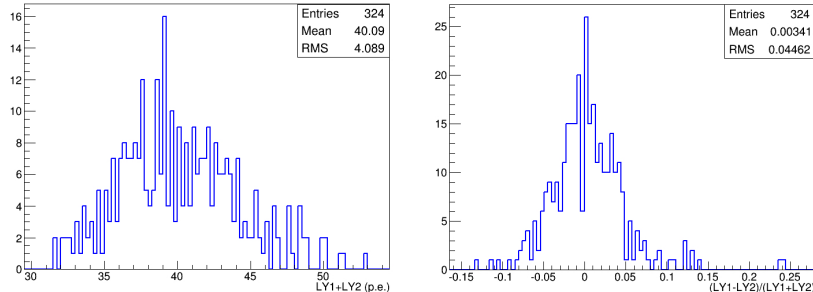


Figure 16: Total light yield distribution (left) and light yield assymetry (right) measured at YNU.

Construction of the Side-MRD modules is scheduled from November 2017 at Yokohama National University. They will then be transported to J-PARC for installation on the B2 floor of the T2K near detector hall.

Same electronics as the WAGASCI modules (see Sec. 2.1.2) are used for the Side-MRD modules.

3 Physics goals

We will measure the differential cross section for the charged current interaction on H₂O and Hydrocarbon(CH)). The water-scintillator mass ratio of the WAGASCI module is as high as 5:1 and the high purity measurement of the cross section on H₂O is possible. One experimental option is to remove water from one of the two WAGASCI modules. The water-out WAGASCI module will allow to measure pure-CH target interactions with very low momentum-threshold for protons. It will also benefit to subtract the background from interaction with scintillator in the water target measurement. Another option is to add the T2K proton module which is fully made of plastic scintillators. It will allow the high statistics comparison of cross section between H₂O and CH and also comparison with the ND280 measurement. The actual configuration will be optimized with detailed MC simulation by 2018 Summer.

Our setup allows the measurements of inclusive and also exclusive channels such as 1- μ , 1- μ 1p, 1- μ 1 π^{\pm} np samples, former two of which are mainly caused by the quasi-elastic and 2p2h interaction and the latter is mainly caused by resonant or coherent pion production and deep elastic scattering. In general, an accelerator produced neutrino beam spectrum

363 is wide and the energy reconstruction somehow rely on the neutrino interaction model.
364 Therefore, recent neutrino cross section measurement results including those from T2K
365 are given as a flux-integrated cross section rather than cross sections as a function of
366 the neutrino energy to avoid the model dependency. We can provide the flux-averaged
367 cross section. In addition, by combining our measurements with those at ND280, model-
368 independent extraction of the cross section for narrow energy region becomes possible.
369 This method was demonstrated in [1] and also proposed by P** (NUPRISM).

370 **3.1 Expected number of events**

371 Expected number of neutrino events after the event selections is evaluated with Monte
372 Carlo simulations as we will discuss in Section 5. In the neutrino-mode, 4.2×10^3 , 1.1×10^3
373 and 3.8×10^3 CC neutrino events are expected in the water-in WAGASCI module, the
374 water-out WAGASCI module and the INGRID proton module after the selections with
375 0.5×10^{21} POT, and its purities are 78.0 %, 97.5 % and $\sim 98\%$. In the antineutrino-mode,
376 1.7×10^3 , 0.4×10^3 and 1.5×10^3 CC antineutrino events are expected in the water-in
377 WAGASCI module, the water-out WAGASCI module and the INGRID proton module
378 after the selections with 0.5×10^{21} POT, and its purities are 59.5 %, 74.4 % and $\sim 74\%$.

379 Statical errors of flux integrated CC-inclusive neutrino cross section measurements on
380 H₂O (full acceptance) and CH targets (forward acceptance) will be 1.5 % and 1.6 % with
381 0.5×10^{21} POT in the neutrino-mode. Statical errors of flux integrated CC-inclusive anti-
382 neutrino cross section measurements on H₂O (full acceptance) and CH targets (forward
383 acceptance) will be 2.4 % and 2.5 % with 0.5×10^{21} POT in the antineutrino-mode.

384 Statical errors of flux integrated H₂O to CH CC-inclusive neutrino cross section ratio
385 measurement will be 3.1 % (full acceptance) and 2.3 % (forward acceptance) with 0.5×10^{21}
386 POT in the neutrino-mode. Statical errors of flux integrated H₂O to CH CC-inclusive
387 antineutrino cross section ratio measurement will be 5 % (full acceptance) and 3.7 %
388 (forward acceptance) with 0.5×10^{21} POT in the antineutrino-mode.

389 **3.2 Pseudo-monochromatic beam by using different off-axis fluxes**

390 The off-axis method gives narrower neutrino spectrum, and the peak energy is lower for
391 larger off-axis angle. There still remains high energy tail mainly due to neutrinos from
392 Kaon decay. The off-axis angle of the WAGASCI location is 1.5 degree and different from
393 the ND280 2.5 degree. Top two plots of Figure 17 show the energy spectra of fluxes and
394 neutrino interaction events at these two different location. The high energy tail of ND280
395 flux can be somehow subtraction by using the WAGASCI measurement. The low energy
396 part of the WAGASCI flux can be also subtracted by using the ND280 measurement.
397 Bottom two plots of Figure 17 demonstrate this method. We can effectively get two fluxes,
398 from 0.2 GeV to 0.9 GeV and 0.6 GeV and 2 GeV and measure flux-integrated cross section
399 for these two fluxes.

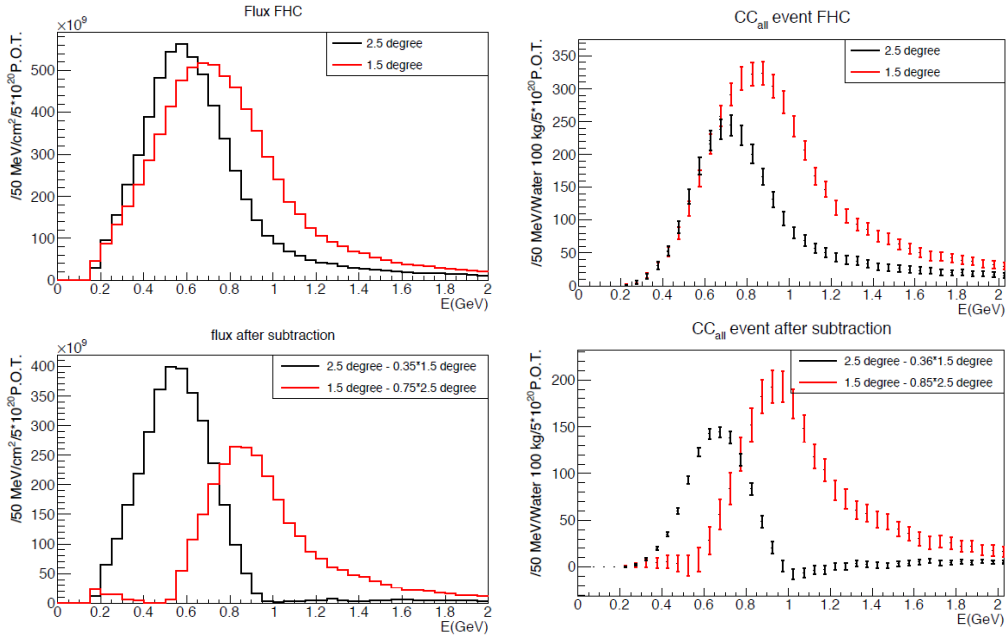


Figure 17: Energy spectra obtained by using different off-axis angle fluxes. Top two plots show the fluxes(left) and spectra of interaction events (right) for ND280 (off-axis 2.5 degree) and WAGASCI (off-axis 1.5 degree). Bottom two plots show the fluxes (left) and spectra of interaction events (right) obtained by subtraction of fluxes at ND280 and WAGASCI. The error bar is for the statistical error and those in the bottom right plot is obtained assuming the statistical error for ND280 measurement is much smaller than that of WAGASCI experiment.

400 Statical errors of flux integrated CC-inclusive neutrino cross section measurements
 401 on H₂O (forward acceptance) and CH targets (forward acceptance) with the pseudo-
 402 monochromatic beam will be 2 % and 1.9 % with 0.5×10^{21} POT in the neutrino-mode.
 403 Statical errors of flux integrated CC-inclusive antineutrino cross section measurements
 404 on H₂O (forward acceptance) and CH targets (forward acceptance) with the pseudo-
 405 monochromatic beam will be 3 % and 2.8 % with 0.5×10^{21} POT in the neutrino-mode.

406 3.3 Subjects WAGASCI can contribute

407 In T2K experiment, neutrinos interact with bound nucleons in relatively heavy nuclei
 408 (Carbon and Oxygen), so the cross-section is largely affected by nuclear effects. The nuclear
 409 effects are categorized as nucleons' momentum distribution in nucleus, interactions with
 410 correlated pairs of nucleons in nucleus (two particles-two holes, 2p2h), collective nuclear

411 effects and final state interactions (FSI) of secondary particles in the nuclei after the initial
 412 neutrino interactions.

413 The 2p2h interactions mainly happen through Δ resonance interactions following a
 414 pion-less decay and interactions with a correlated nucleon pair. The 2p2h interactions are
 415 observed in electron scattering experiments [6] where the 2p2h events observed in the gap
 416 between Quasi-Elastic region and Pion-production region as shown in Figure 18. Neutrino
 417 experiments also attempt to measure the 2p2h interactions, but separation of the QE peak
 418 and the 2p2h peak is more difficult because transferred momentum (p) and energy (w)
 419 are largely affected by neutrino energies which cannot be determined event-by-event in the
 420 wide energy spectrum of the accelerator neutrino beam. Our model-independent narrow
 421 neutrino spectra extracted from combined analyses of our data and ND280 data are ideal
 422 for searching the 2p2h interaction because clearer separation of the QE peak and the 2p2h
 423 peak is expected. Another way to observe the 2p2h interaction is direct measurement of
 424 proton tracks in CC0 π sample with low detection threshold and full acceptance. Figure 19
 425 shows proton multiplicities after FSI in CCQE events and 2p2h events, and Figure 19 shows
 426 opening angles among two proton tracks in the same samples. The water-out WAGASCI
 427 can provide good sample for the 2p2h interaction search because its low density medium
 428 enables the detection of low momentum protons in addition to the full acceptance.

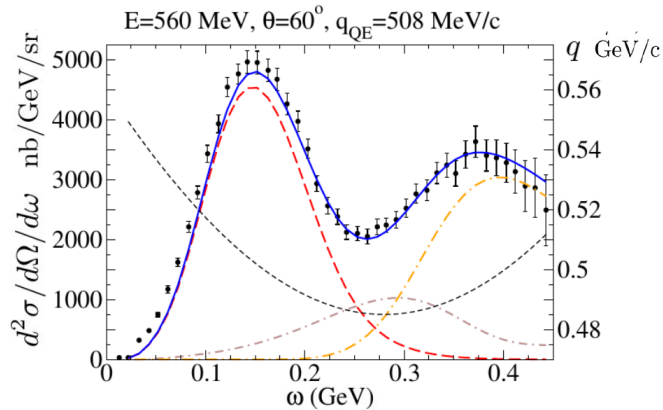


Figure 18: Comparison of inclusive $^{12}\text{C}(\text{e},\text{e}')$ cross sections and predictions of the QE-SuSAv2 model (long-dashed red line), 2p-2h MEC model (dot-dashed brown line) and inelastic-SuSAv2 model (long dot-dashed orange line) (from Ref. [6]). The sum of the three contributions is represented with a solid blue line. The q dependence with ω is also shown (short-dashed black line.)

429 There are various models which describe the collective nuclear effects [7]. The Q^2
 430 dependence of the effects can be tested by measuring angular distribution of muons in
 431 CC1- μ and CC1- $\mu 1\mu$ events. The uncertainties of the effects in low (high) Q^2 regions can

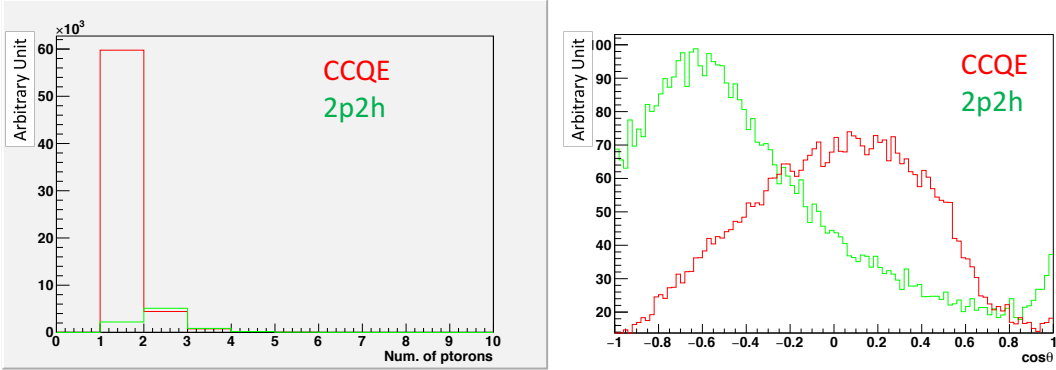


Figure 19: Proton multiplicities (left) and opening angles among two proton tracks (right) after FSI in CCQE events and 2p2h events.

432 be constrained by observing the events with a forward-going (high-angle) muon, so it is
433 essential to measure muon tracks with full acceptance.

434 T2K experiment is starting to use ν_e CC1 π events for its CP violation search to increase
435 the statistics. One of the biggest uncertainty of the CC1 π sample comes from the final
436 state interactions of pions in the nuclei after the initial neutrino interactions because they
437 change the multiplicity, charge and kinematics of the pions. The multi-pion production
438 events can be migrated into the CC1 π sample due to the FSIs, and they become important
439 backgrounds. We can constrain the uncertainties from the pion FSIs by measuring pion
440 rescattering in the detector and pion multiplicity in ν_μ CCn π sample with low detection
441 threshold and full acceptance for pion tracks. The water-out WAGASCI can provide good
442 sample for the pion FSI studies because its low density medium enables the detection of
443 low momentum pions in addition to the full acceptance.

444 4 Status of J-PARC T59 experiment

445 We had submitted a proposal of a test experiment to J-PARC in April 2014 to test a new
446 detector with a water target, WAGASCI, at the neutrino monitor hall, and the proposal
447 was approved as J-PARC T59. The project contains the side and downstream muon range
448 detectors as well.

449 The first WAGASCI module has been constructed in 2016 and installed at the on-
450 axis position in front of the T2K INGRID detector for the commissioning and the first
451 cross section measurement as a part of the T2K experiment. The INGRID electronics
452 boards are used to read the signal. The light yield measured with muons produced by
453 the interaction of neutrinos in the hall wall, shown in Figure 20, is sufficiently high to get

good hit efficiency. A track search algorithm based on the cellular automaton has been

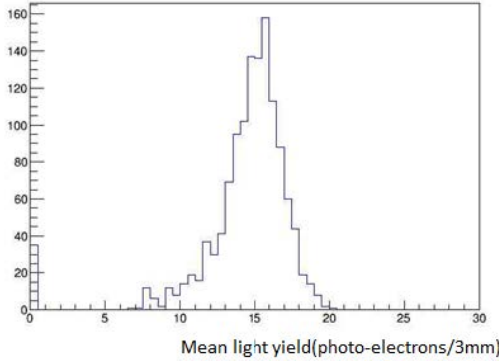


Figure 20: Light yield for muons produced by the interaction of neutrinos in the hall wall. Average light yields for each channel are plotted.

454 developed using the software tools by the T2K INGRID. Examples of observed events are
455 shown in Figure 21 The tracking efficiency in 2-dimensional projected plane was evaluated
456 by comparing the reconstructed track in the WAGASCI module and the INGRID module
457 and shown in Figure22. Note that that the tracking efficiency for high angle (> 70 deg)
458 is not evaluated because of the acceptance of the INGRID module, not because of the
459 limitation of the WAGASCI module.
460

461 In 2017 Autumn, the construction of the second WAGASCI module and the dedicated
462 electronics board were completed. The module and the electronics were install to the B2
463 floor together with the T2K proton module and the INGRID module as shown in Figure 23.
464 The proton module is to be used as the entering muon veto and also for the comparison
465 of interaction between CH and Water. The INGRID module is for the temporary muon
466 detector with limited acceptance for this period. The detector was commissioned and is
467 in operation to take data with the antineutrino beam during the T2K beam time from
468 October.

469 The production of the components of the side muon range detectors has been completed
470 and now the detectors are being assembled at the Yokohama National University. These
471 detectors will be installed sometime from January to June, 2018 when T2K is not running.

472 The Baby MIND detector was transported from CERN to Japan in December, 2017.
473 It will be installed and commissioned in Jan.-Feb. 2018 and T59 will take the neutrino-
474 induced muon data in April and May.

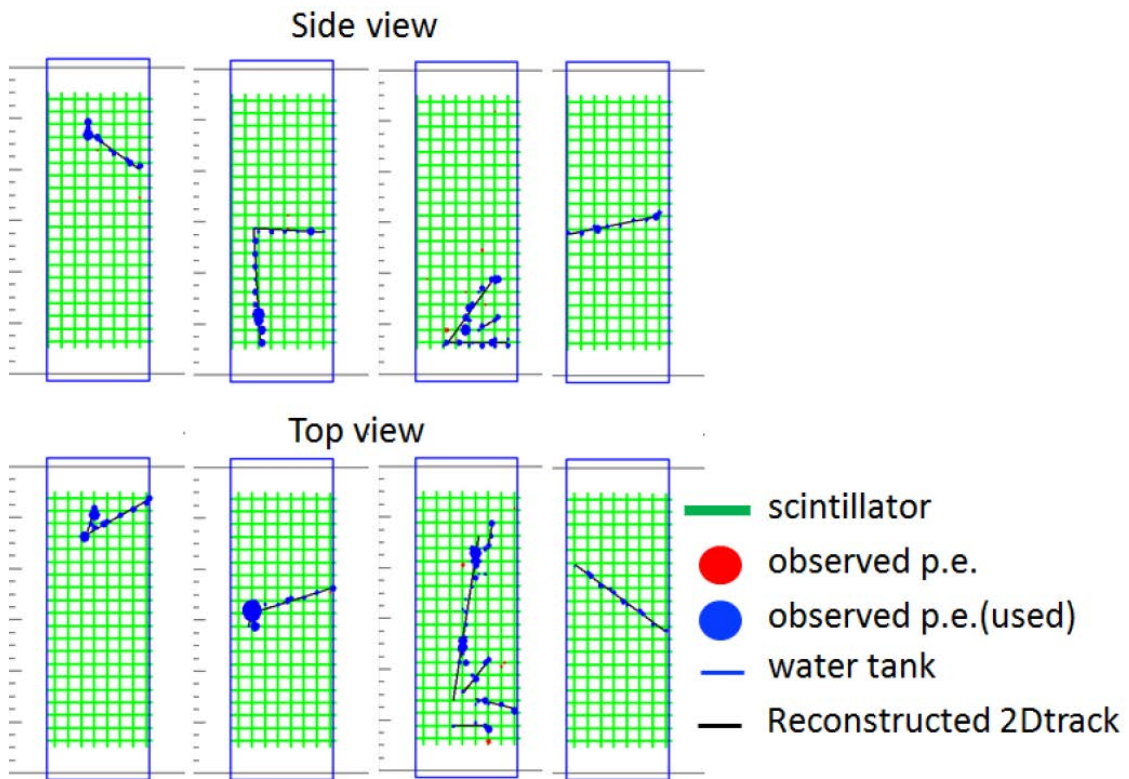


Figure 21: Example event displays of the WAGASCI module at on-axis. The reconstructed tracks are overlaid.

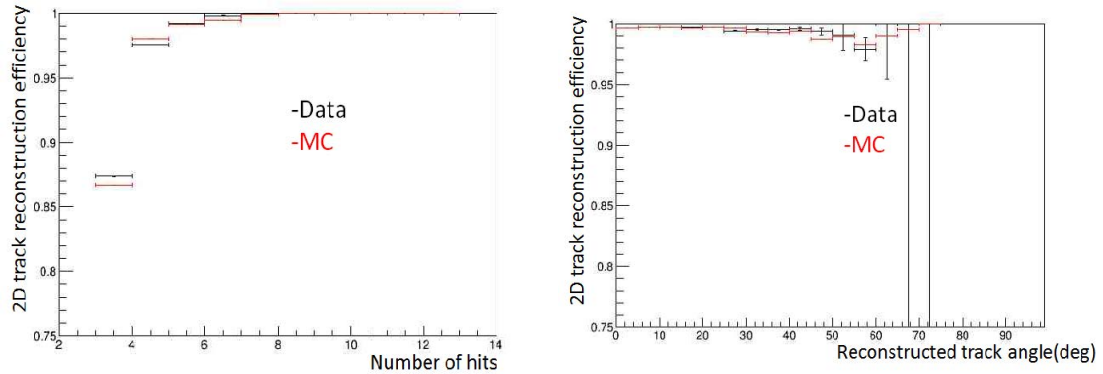


Figure 22: 2D track reconstruction efficiency as a function of number of hits (left) and track angle (right). Here the track angle is the one reconstructed by the INGRID module.

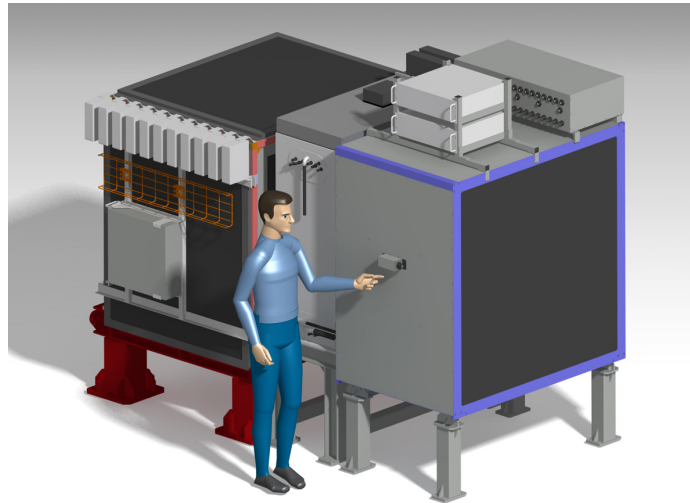


Figure 23: J-PARC T59 detector configuration in October 2017.

475 **5 MC studies**

476 **5.1 Simulation setup**

477 Simulation study was conducted by using the T2K neutrino flux generator, JNUBEAM,
478 neutrino interaction simulator, NEUT, and Geant4 for the detector responses.

479 The detector geometry in the simulation so far is different from the actual setup as
480 shown in Figure 24. The active neutrino target region consists of four WAGASCI modules.
481 The size of the WAGASCI module is same as the actual one: 100 cm × 100 cm in the
482 x and y directions and 50 cm along the beam direction (z-direction). Two Side-MRD
483 modules is installed at both sides of the WAGASCI modules, and each Side-MRD module
484 consists of ten iron plates whose dimension is 3 cm (thickness) × 200 cm (height) × 320 cm
485 (width). The distance between the Side-MRD modules and WAGASCI modules is 80 cm.
486 The downstream-MRD is equivalent to the Baby-MIND, but without the magnetic field.
487 It consists of thirty iron plates whose dimension is 3 cm (thickness) × 200 cm (height)
488 × 400 cm (width). The distance between the downstream-MRD modules and WAGASCI
489 modules is 80 cm. Update of the study with the actual geometry is now underway.

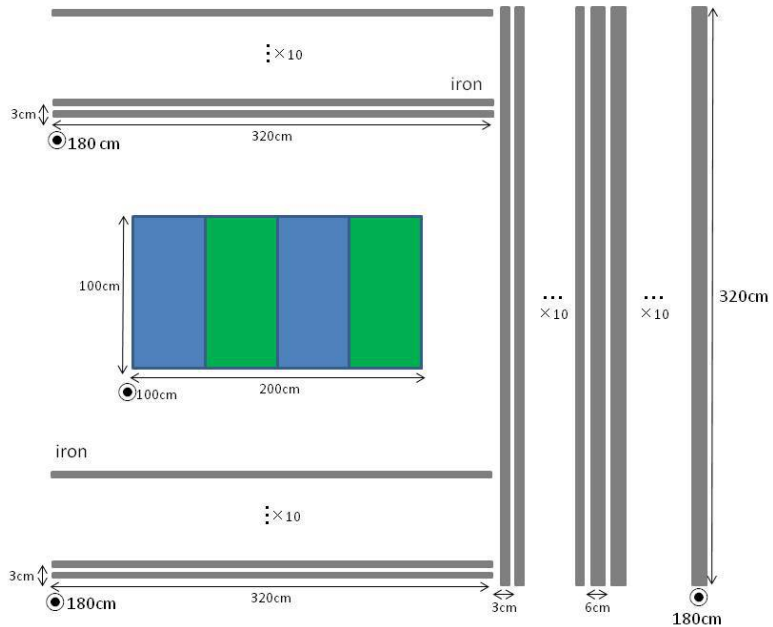


Figure 24: Geometry of the detectors in the Monte Carlo simulation.

490 To simulate the signal, the energy deposit inside the scintillator is converted into the

491 number of photons. The effects of collection and attenuation of the light in the scintillator
492 and the WLS fiber are simulated, and the MPPC response is also taken into account. The
493 light yield is smeared according to statistical fluctuations and electrical noise.

494 **5.2 Event selection**

495 Tracks are reconstructed in two-dimensional planes in each sub-detector. Then, track
496 matching among the sub-detectors and three-dimensional track reconstruction are per-
497 formed. These analysis tools have been developed from the software tools by the T2K
498 INGRID and in mature stage already.

499 The events are selected as follows. The starting point of the track is required to be
500 5 cm away from the edge of the WAGASCI module. This is to remove the background
501 from the outside. The longest track has to penetrate more than one (five) iron plates in
502 Side-MRD modules (Baby-MIND). This cut select a muon track and rejects backgrounds
503 from NC and neutral particles. Then, in order to determine the muon momentum, it is
504 required that the longest track stops in MRDs (Side-MRD modules and Baby-MIND) or
505 penetrate all iron plates.

506 Table 1 shows numbers of the selected events in one water-in WAGASCI module after
507 the event selection. We expect 4,239 (1,666) events from charged-current interaction on
508 water with 5×10^{20} POT in (anti)neutrino-mode with one water-in WAGASCI module.
509 The purity, when interactions on CH is counted as background, is 78% for the neutrino-
510 mode. There is a significant contamination from the wrong-sign (neutrino) interaction for
511 antineutrino-mode, however, we expect that it will be removed with efficiency higher than
90% by Baby MIND.

Table 1: Expected number of the selected neutrino-candidate events in one water-in WA-
GASCI module with 5×10^{20} POT in each of neutrino-mode and antineutrino-mode. Note
that the wrong sign component will be reduced by one order by applying the charge selec-
tion by Baby MIND.

	CC on water	NC on water	Interaction on CH	wrong sign interaction
ν -mode	4239	107	1087	(negligible)
anti- ν -mode	1666	14	560	(561)

512
513 Table 2 and 3 summarize contributions classified by the interaction types and final state
514 topologies for the selected charged current-interaction events, respectively.

515 Figure 25 shows the reconstructed angles of the longest tracks in the selected events in
516 the neutrino-mode and the anti-neutrino mode. Figure ?? shows the iron plane numbers
517 in Side-MRD and Baby-MIND corresponding to the end points of the longest tracks in the
518 selected events in the neutrino-mode and the anti-neutrino mode.

Table 2: Interaction types for the selected charged-current events.

	CCQE	2p2h	CC resonant π	CC-DIS
ν -mode	48.4 %	9.7 %	27.1 %	14.7 %
anti- ν -mode	57.1 %	8.2 %	17.3 %	17.3 %

Table 3: Final state topologies for the selected charged-current events.

	CC0 π	CC1 π	CC2 π	CCn π
ν -mode	67.4 %	20.9 %	3.0 %	8.7 %
anti- ν -mode	79.5 %	16.3 %	1.2 %	3.0 %

519 6 Standalone WAGASCI-module performances

520 In the previous sections, the WAGASCI detector was studied using the Muon Range Detectors. In this section, the standalone abilities of WAGASCI module are presented. Using
 521 the WAGASCI configuration presented in Section 5, we have evaluated that only 7% of
 522 the muons will be stopped in one of the WAGASCI modules. However, this proportion
 523 increases to 53% for pions and 73% for protons produced by neutrino interactions at 1.5°
 524 off-axis. Figure 27 shows the momentum distribution of these daughter particles as well as
 525 for the sub-sample stopped in one of the WAGASCI modules. Therefore, the study of the
 526 standalone abilities of the WAGASCI module in this section are dominantly motivated by:
 527

- 528 • the accurate measurement of the neutrino interaction final states. Though most of the
 529 muons will be reconstructed and identified in the MRDs, the hadronic particles will
 530 predominantly stops in one WAGASCI module. One has therefore to rely exclusively

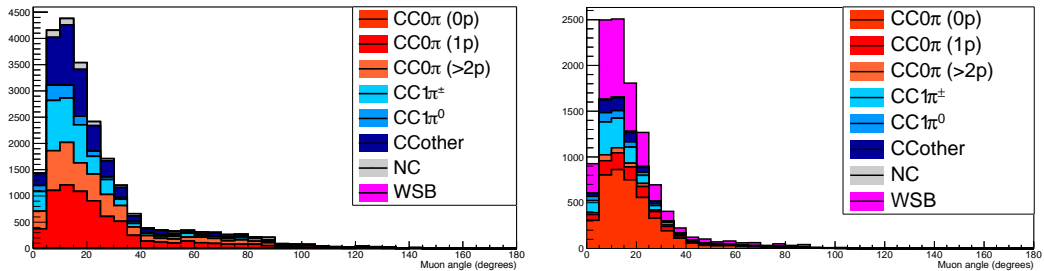


Figure 25: The reconstructed angles of the longest tracks in the selected events in the neutrino-mode (left) and the antineutrino-mode (right).

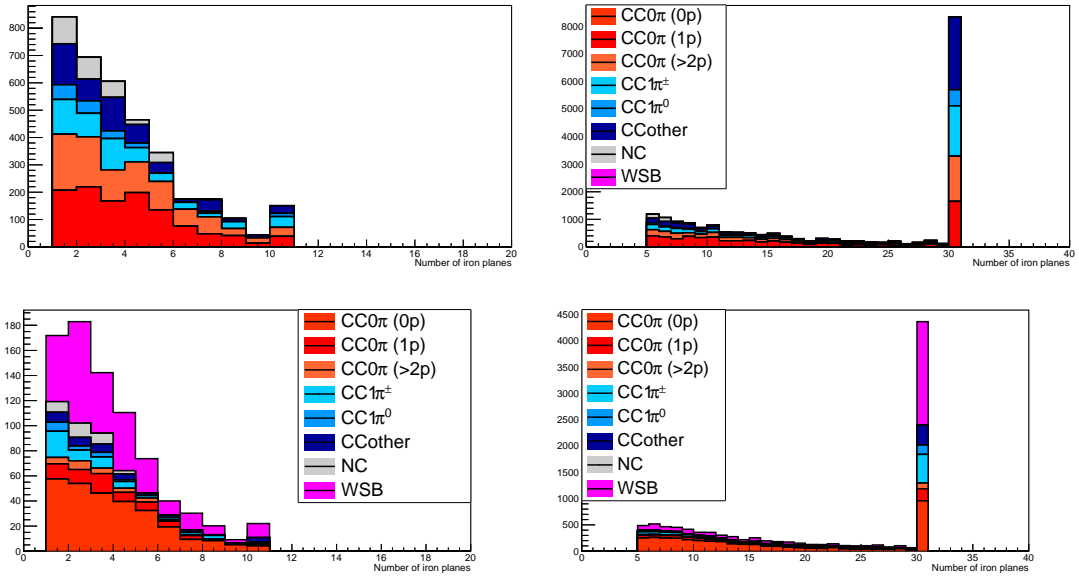


Figure 26: Iron plane numbers in Side-MRD (left) and Baby-MIND (right) corresponding to the end points of the longest tracks in the selected events in the neutrino-mode (top) and the antineutrino-mode (bottom).

531 on the WAGASCI module information alone to reconstruct, identify and measure the
 532 momentum of pions or protons.

- 533 • the coverage of the MRDs is not 4π . Using the WAGASCI module information can
 534 therefore help to constraint the particles that exits the WAGASCI module but do
 535 not geometrically enters any MRD.
- 536 • the particle identification of low momenta muons $p_\mu < 300 \text{ MeV}/c$ that will leave only
 537 few hits in the MRD. Using the WAGASCI module information will clearly enhance
 538 the particle identification.

539 This study is based on an original study done for the ND280 upgrade target, with some
 540 modifications. Though the cell size is similar to the WAGASCI configuration presented
 541 in Section 5, the external dimensions are different ($186.4 \times 60 \times 130 \text{ cm}^3$). Whenever the
 542 results are presented with this external size and this parameter is likely to impact the
 543 result, it will be mentioned.

544 Note that in this section, a simplified reconstruction algorithm presented in Section 6.1 is
 545 used. The fiducial volume is chosen accordingly as the inner cube of the module which
 546 surfaces are distant of $4 \times$ scintillator space = 10 cm from the module external surfaces.

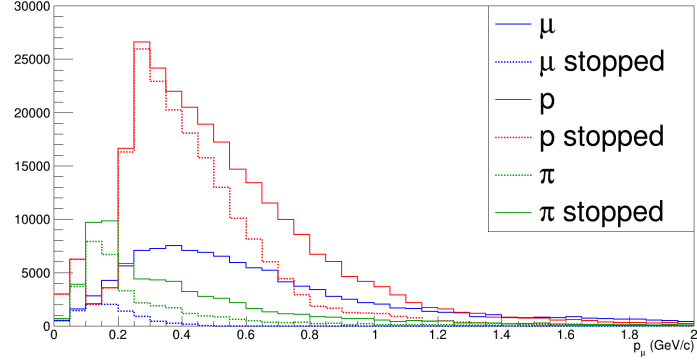


Figure 27: Momentum distribution of true particles in WAGASCI (plain) and corresponding distributions only for particles stopping into the WAGASCI module (dashed).

547 The neutrino interactions are simulated using NEUT v5.3.2. The NEUT input neutrino
 548 flux is estimated using JnuBeam v13a and assuming the detector to be located at 1.5°
 549 off-axis, as in Section 5. Note that the event reconstruction efficiency as a function of true
 550 neutrino energy might be changed at 1.5° , due for example to different Q^2 distributions. For
 551 this reason, one has to note that the reconstruction results might slightly be changed from
 552 2.5° and 1.5° . To avoid a similar change on the particle-only reconstruction efficiencies,
 553 they will be presented as a function of variables that completely characterize the particle
 554 kinematic state, *i.e.* its momentum and angle. Figure 28 shows the vertices distributions
 555 of the daughter particles of neutrinos interacting one standard WAGASCI water-module.
 556 In this section, we will show the detector reconstruction and particle identification in this
 557 phase space, both for leptonic and hadronic particles. We will finally show an empty
 558 WAGASCI module can highly enhance the ability to constrain the neutrino interaction
 559 final state which is critical to reduce the corresponding uncertainties.

560 6.1 Reconstruction algorithm

561 6.1.1 Description

562 For this section, an ideal “simulated” reconstruction is developed. A particle is recon-
 563 structed if:

- 564 1. The particle is charged.
- 565 2. Lets at least one hit (energy deposit > 2.5 photo-electron) in a scintillator.
- 566
- 567 3. The particle enters one TPC and let one hit in the tracker.

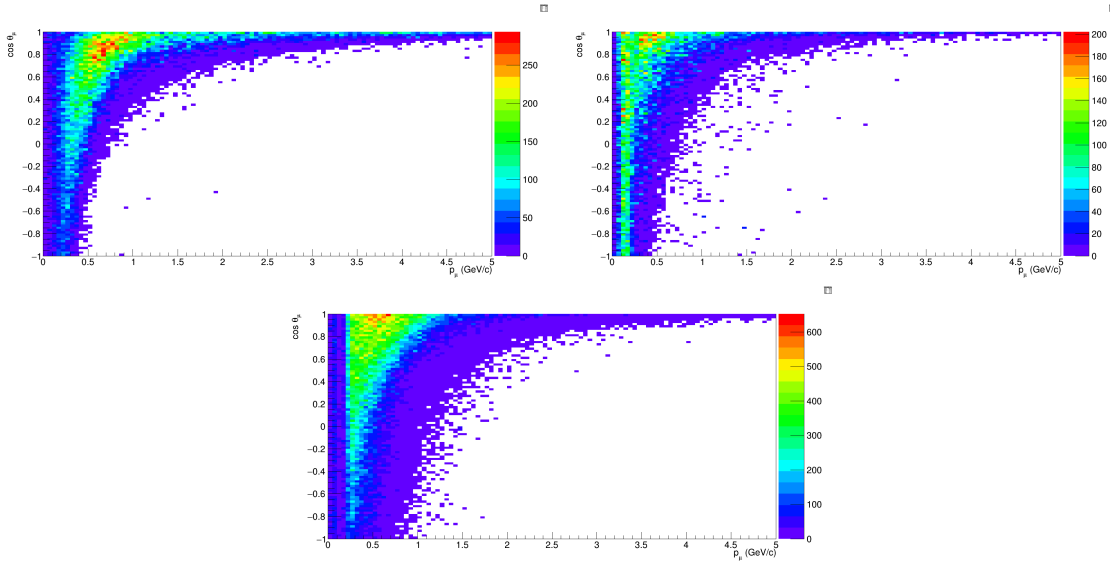


Figure 28: True number of muons (left), charged pions (right) and protons (bottom) in the two WAGASCI water-module as a function of the particles momenta and angles at 1.5° .

568 Or

569

570

- The particle should be long enough to be reconstructed by the detector in at least 2 out of 3 views (XZ, YZ, XY). The length criterion requires the particle to let at least 4 hits in the detector. In the “less favourable case” of pure longitudinal or transverse going tracks, it represents a the track length of $L_{track} \geq 4 \times$ scintillator space = 10.0 cm.
- In the views where particles pass the length criterion, the particle shall not be superimposed with longer tracks in at least two views. The superposition criterion is estimated with the distance inter-tracks (DIT) which corresponds to the orthogonal distance between two tracks at the ending point of the shortest one (see Figure 29). For a track 1, the superposition criterion is tested with every longer tracks that starts at the same vertex. Let \vec{p}_1^a the vector of track 1, and p_1^a its projections in the XZ, YZ and XY planes respectively for $i=1,2,3$. Note that these are projections in a 2D planes and not on a direction vector. In this case, the relative angle between the track 1 and a longer track 2 (of vector \vec{p}_2^a) in a view a is given by:

$$\cos \theta = \frac{\vec{p}_1^a \cdot \vec{p}_2^a}{\|\vec{p}_1^a\| \|\vec{p}_2^a\|} \quad (1)$$

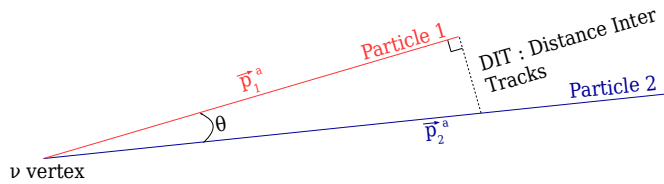


Figure 29: Definition of the distance inter tracks.

585 and the distance inter track is given by:

$$\text{DIT} = \|\vec{p}_1^a\| \sin \theta \quad (2)$$

586 The DIT should be higher than $4 \times$ scintillator width for the track 1 to be not
 587 superimposed with the track 2 in the view a, which also corresponds to 10.0 cm
 588 in the nominal configuration.

589 **6.1.2 Performances**

590 The particle-only reconstruction efficiencies and the reconstruction threshold in momenta
 591 are shown in Table 4. This threshold is defined as the maximal momentum for which the
 592 reconstruction efficiency is smaller than 30%. The thresholds in muon and pion momenta
 593 are 150 MeV/c. Most of the muons are above this threshold (see Figure 28) which leads
 594 to a 79% reconstruction efficiency.

	μ	π	p
Reconstruction Efficiency	79%	52%	26%
Momentum threshold	150 MeV/c	150 MeV/c	550 MeV/c

Table 4: Reconstruction efficiency and momentum threshold for muons, pions and protons.
 The threshold is defined as the maximal momentum for which particles have a reconstruction efficiency smaller than 30%.

595 The lower pion and proton efficiencies (respectively 52% and 26%) are due to lower
 596 efficiencies for similar momenta than muons, coming from strong interactions as shown
 597 on Figures 30. Efficiencies of each particle type tend to decrease in the backward region
 598 due to particle lower momenta. However, for a fixed momentum value, the reconstruc-
 599 tion efficiency is almost uniform which confirms the ability of the WAGASCI detector to
 600 reconstruct high angle tracks.

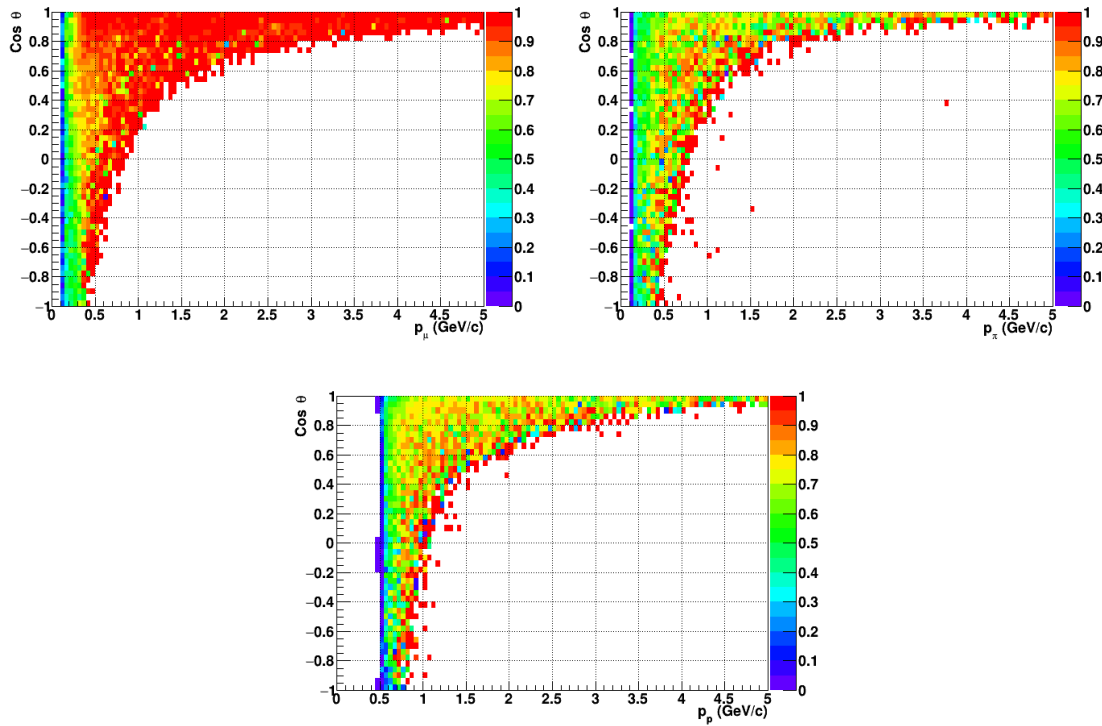


Figure 30: Reconstruction efficiency of muons (left), charged pions (right) and protons (bottom) in the WAGASCI water-module as a function of the particles momenta and angles.

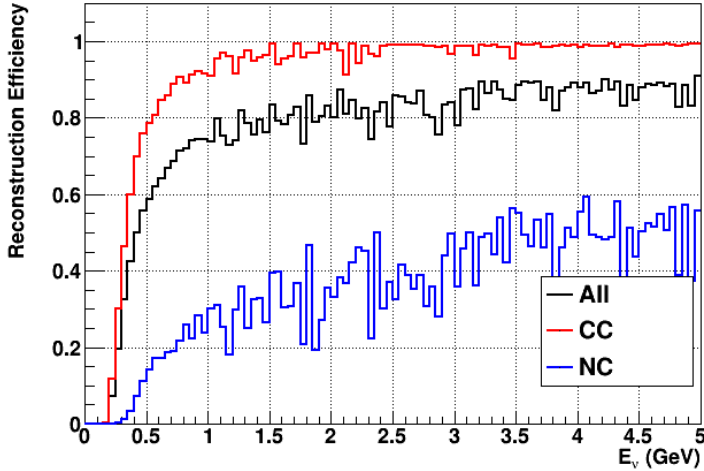


Figure 31: Reconstruction efficiency of all neutrino (black), CC (red) and NC (blue) interactions in the WAGASCI water-module as a function of the neutrino energy.

601 The reconstruction is thereafter tested on neutrino events. Table 5 summarizes the
 602 number of reconstructed events and efficiencies for each interaction type. As expected
 603 from the high muon reconstruction efficiency, the charged current interactions have recon-
 struction efficiencies $\geq 85\%$.

	CC0 π	CC1 π	CCOthers	NC	All
Reconstruction efficiency	85%	87%	91%	22%	68%

Table 5: Number of true interactions reconstructed. The purity and reconstruction effi-
 ciency of each true interaction is also shown.

604
 605 The reconstruction efficiencies as a function of the neutrino energy and muon kinematics
 606 are respectively shown on Figure 31 and 32.

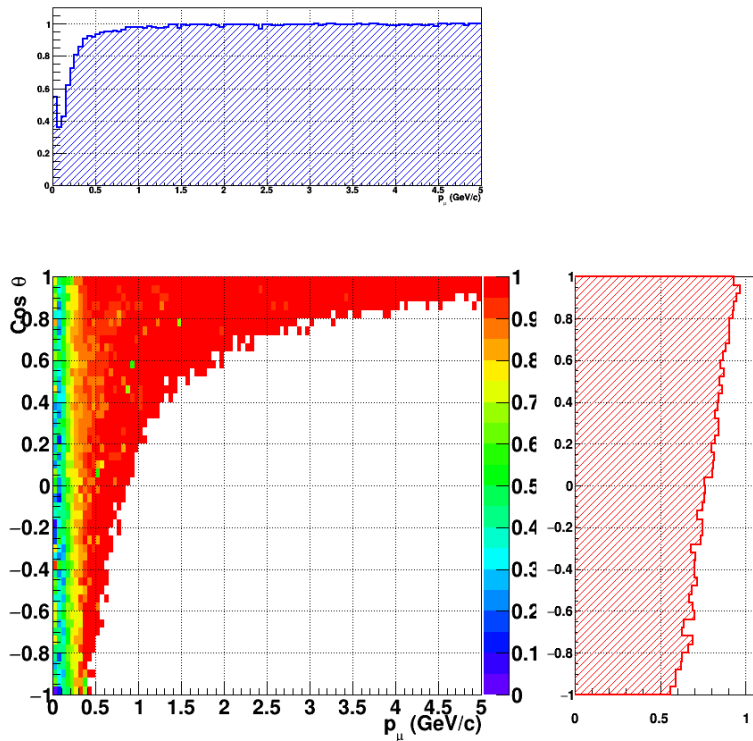


Figure 32: Reconstruction efficiency of CC interactions in the WAGASCI water-module as a function of the muon kinematic variables (momentum and angle).

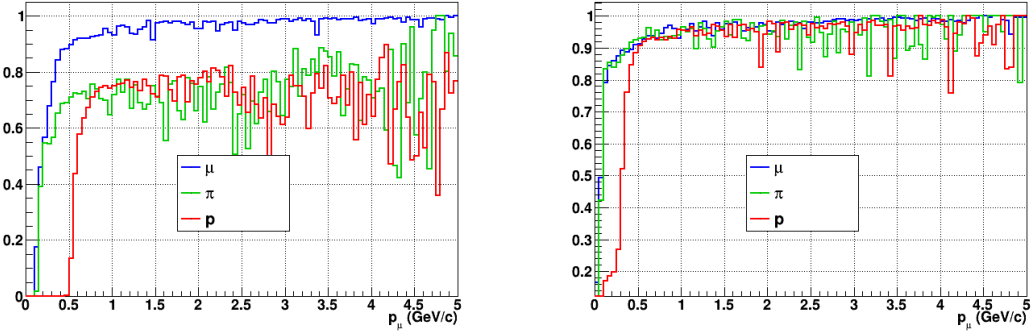


Figure 33: Reconstruction efficiency for muons, pions and protons in the water-in (left) and water-out (right) modules.

607 Note that a Particle Identification Algorithm has been also developed. It is based on
 608 the charge deposition of the particles in the scintillator, of the detection of a decay-electron.
 609 However, this information highly depends on the number of scintillator hit by a particle,
 610 which creates an important difference between a real WAGASCI module and the one used
 611 for the ND280-upgrade simulation. For this reason, the corresponding results will not be
 612 detailed here, but can be found in [?].

613 6.2 Background subtraction: the water-out module

614 In the nominal configuration, 20% of the neutrino interactions occurs on scintillators
 615 (C_8H_8). This background should be removed in order to measure the neutrino interac-
 616 tion on the same target as Super-K, which suppress the differences in cross-section models.
 617 For this purpose, we propose to use a water-out module, where the water is replaced by
 618 air. The detector is therefore fully active and has a 3 mm spatial resolution (scintillator
 619 thickness) which create an ideal detector to reconstruct and identify hadrons, and study
 620 np-nh interactions. The counter-part is the difference in particle energy deposition between
 621 the water and this water-out module that will need to be corrected for. In this section,
 622 we present the capabilities of such a module, and the impact it can have on cross-section
 623 measurements for the neutrino community in general and T2K in particular.
 624 The same reconstruction and selection as the water-in module is applied. Figure 33 shows
 625 the comparison between the water-in and the water-out reconstruction efficiencies for muon,
 626 pions and protons. 90% of the muons and 87% of the pions are reconstructed, while 70%
 627 of the protons are even reconstructed. It allows to lower down the proton threshold to
 628 250 MeV/c (see Table 6).

629 As a consequence of tracking even low momenta particle, the reconstruction efficiency
 630 is uniform and almost maximal on the entire $\cos \theta_\mu$ phase space, as shown on Figure 34.

	μ	π	p
Reconstruction Efficiency Momentum threshold	90% 50 MeV/c	87% 50 MeV/c	70% 250 MeV/c

Table 6: Reconstruction efficiency, proportions of μ -like and non μ -like and momentum threshold for muons, pions and protons in the empty module. The threshold is defined as the maximal momentum for which particles have a reconstruction efficiency smaller than 20%.

631 Since the fiducial mass represents 0.25 tons, the total number of events is divided by a
 632 factor of 3 compared to the water-in module. The water-out module offers interesting
 633 possibilities to study np-nh interaction since 70% of the protons are reconstructed. In the
 634 future, a possible separation as a function of the number of proton track will be studied.
 635 Moreover, we are currently pursuing the use of single and double transverse variables (cite
 636 Xianguo) to open new possibilities for separating np-nh from Final State Interactions, or
 637 for isolating the interactions on hydrogen from interactions on carbon in this module.

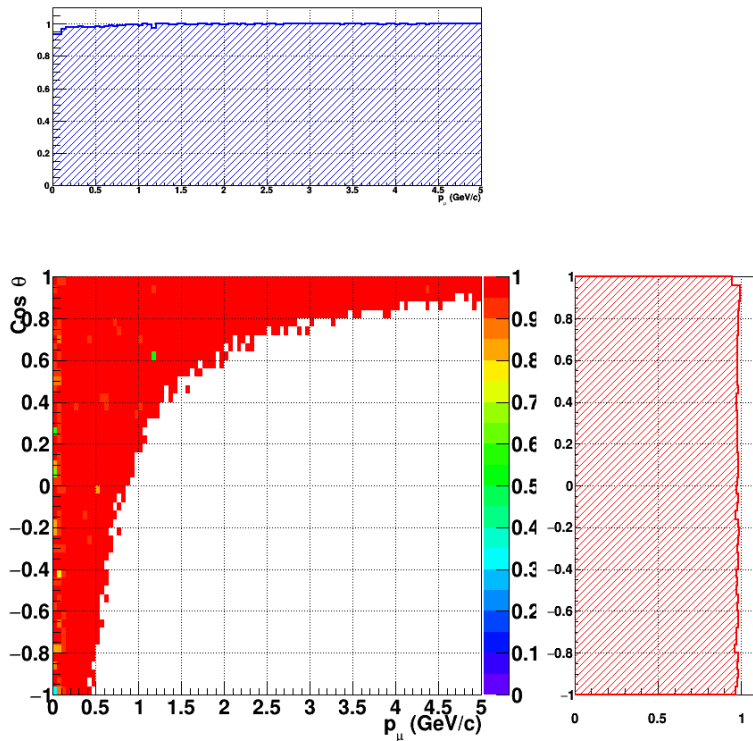


Figure 34: Reconstruction efficiency of CC interactions in the WAGASCI empty module as a function of the muon kinematic variables (momentum and angle).

638 **7 Schedule**

639 We would like to start a physics data taking from T2K beam time after the summer
640 shutdown in 2018. By then, commissioning and tests of the detectors will be completed
641 in J-PARC T59. The experiment can run parasitically with T2K, therefore we request no
642 dedicated beam time nor beam condition as discussed in the following section.

643 Once the approved POT is accumulated, the WAGASCI modules will be removed
644 from the experimental site, but we would like to keep the Baby-MIND and the Side-MRD
645 modules on the B2 floor of the NM pit as common platforms of future neutrino experiments
646 using the T2K neutrino beam.

647 **8 Requests**

648 **8.1 Neutrino beam**

649 The experiment can run parasitically with T2K, therefore we request no dedicated beam
650 time nor beam condition. As data taking periods, we request the ‘nominal’ T2K one-year
651 operation both for the neutrino beam and the antineutrino beam. The T2K has been
652 requesting 0.9×10^{21} POT/year and actually accumulating about 0.7×10^{21} POT/year in
653 recent years. For each year, starting from the Autumn, T2K is running predominantly in
654 the neutrino mode or in the antineutrino mode. Our request is to have one-year neutrino-
655 mode data and another one-year antineutrino mode data assuming that the POT for the
656 fast extraction in each year is more than 0.5×10^{21} POT.

657 **8.2 Equipment request including power line**

658 We request the followings in terms of equipment on the B2 floor:

- 659 • Site for the WAGASCI modules, Side-MRD modules and BabyMIND and their elec-
660 tronics system on the B2 floor of the near detector hall (Figure 2 and 3).
- 661 • Anchor points (holes) on the B2 floor to secure the WAGASCI modules, Side-MRD
662 module and Baby-MIND, detailed floor plans to be communicated in a separate
663 document.
- 664 • Power line for the magnets in Baby-MIND: 400 V tri-phase 48-to-62 Hz, capable of
665 delivering 12 kW. We have a wish for the magnet power line to be installed and
666 available to us by beginning of March 2018.
- 667 • Electricity for electronics and water circulation system, 3 kW, standard Japanese
668 electrical sockets.

- 669 1. Online PCs: 2.1 kW

670 2. Electronics: 0.7 kW

671 3. Water sensors: 1 kW

- 672 • Air conditioner for cooling heat generation at Baby-MIND magnets, online PCs and
673 electronics
- 674 • Beam timing signal and spill information
- 675 • Network connection

676 The infrastructure for much of the above exists already. Exceptions are the power line
677 for the magnet and the electronics and holes in the B2 floor to anchor the detector support
678 structures.

679 References

- 680 [1] K. Abe et al. Measurement of the muon neutrino inclusive charged-current cross
681 section in the energy range of 13 GeV with the T2K INGRID detector. *Phys. Rev.*,
682 D93(7):072002, 2016.
- 683 [2] M. Antonova et al. Baby MIND Experiment Construction Status. In *Prospects in*
684 *Neutrino Physics (NuPhys2016) London, London, United Kingdom, December 12-14,*
685 2016, 2017.
- 686 [3] K. Nitta et al. The k2k scibar detector. *Nucl. Instrum. Meth. A*, 535:147, 2004.
- 687 [4] F. Magniette F. Gastaldi, R. Cornat and V. Boudry. A scalable gigabit data acquisition
688 system for calorimeters for linear collider. *proceedings of TIPP2014*, page PoS 193,
689 2014.
- 690 [5] J. Fleury, S. Callier, C. de La Taille, N. Seguin, D. Thienpont, F. Dulucq, S. Ahmad,
691 and G. Martin. Petiroc and Citiroc: front-end ASICs for SiPM read-out and ToF
692 applications. *JINST*, 9:C01049, 2014.
- 693 [6] M. B. Barbaro J. A. Caballero T. W. Donnelly G. D. Megias, J. E. Amaro. Inclusive
694 electron scattering within the susav2 meson-exchange current approach. *Phys. Rev.*
695 D, 94:013012, 2016.
- 696 [7] M. Valverde J. Nieves, J. E. Amaro. Inclusive quasi-elastic neutrino reactions. *Phys.*
697 *Rev. C*, 70:055503, 2004.
- 698 [8] Yu. G. Kudenko, L. S. Littenberg, V. A. Mayatsky, O. V. Mineev, and N. V. Ershov.
699 Extruded plastic counters with WLS fiber readout. *Nucl. Instrum. Meth.*, A469:340–
700 346, 2001.

- 701 [9] O. Mineev, Yu. Kudenko, Yu. Musienko, I. Polyansky, and N. Yershov. Scintillator
702 detectors with long WLS fibers and multi-pixel photodiodes. *JINST*, 6:P12004, 2011.
- 703 [10] Etam Noah et al. Readout scheme for the Baby-MIND detector. *PoS*, Pho-
704 toDet2015:031, 2016.
- 705 [11] Omega. Spiroc 2 user guide. 2009.